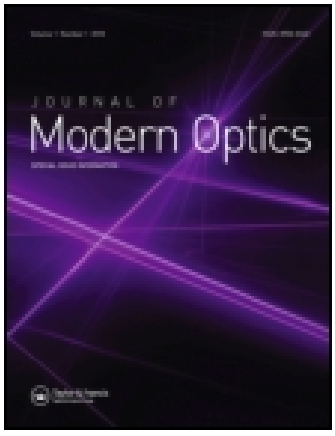

Journal of Modern Optics
Publication details, including instructions for authors and subscription information:
http://www.tandfonline.com/loi/tmop20

Ultrafast optical Kerr gate of bismuth-plumbum oxide glass for time-gated ballistic imaging

Shichao Xu[a], Jinhai Si[a], Wenjiang Tan[a], Pinping Zhan[a], Yongze Yu[b], Jianrong Qiu[b], Feng Chen[a] & Xun Hou[a]

[a] Key Laboratory for Physical Electronics and Devices of the Ministry of Education & Shaanxi Key Lab of Information Photonic Technique, School of Electronic and Information Engineering, Xi'an Jiaotong University, Xi'an, China

[b] State Key Laboratory of Luminescent Materials and Devices, Institute of Optical Communication Materials, South China University of Technology, Guangzhou, China

Published online: 28 Jul 2014.

To cite this article: Shichao Xu, Jinhai Si, Wenjiang Tan, Pinping Zhan, Yongze Yu, Jianrong Qiu, Feng Chen & Xun Hou (2014) Ultrafast optical Kerr gate of bismuth-plumbum oxide glass for time-gated ballistic imaging, Journal of Modern Optics, 61:17, 1452-1456, DOI: 10.1080/09500340.2014.940018

To link to this article: http://dx.doi.org/10.1080/09500340.2014.940018

Journal of Modern Optics, 2014
Vol. 61, No. 17, 1452–1456, http://dx.doi.org/10.1080/09500340.2014.940018

Ultrafast optical Kerr gate of bismuth–plumbum oxide glass for time-gated ballistic imaging

Shichao Xu[a], Jinhai Si[a], Wenjiang Tan[a]*, Pinping Zhan[a], Yongze Yu[b], Jianrong Qiu[b], Feng Chen[a] and Xun Hou[a]

[a]*Key Laboratory for Physical Electronics and Devices of the Ministry of Education & Shaanxi Key Lab of Information Photonic Technique, School of Electronic and Information Engineering, Xi'an Jiaotong University, Xi'an, China;* [b]*State Key Laboratory of Luminescent Materials and Devices, Institute of Optical Communication Materials, South China University of Technology, Guangzhou, China*

(*Received 19 March 2014; accepted 25 June 2014*)

We demonstrated the time-gated ballistic imaging technique using a femtosecond optical Kerr gate (OKG) of bismuth–plumbum oxide glass, the nonlinear optical properties of which were also investigated. The third-order nonlinear refractive-index n_2 of the bismuth–plumbum oxide glass was measured to be 2.19×10^{-15} cm^2/W, and the nonlinear response time was estimated to be shorter than 180 fs. For the time-gated ballistic imaging, the maximum measurable optical density of turbid media using the OKG of bismuth–plumbum oxide glass was 9.3, while only 7.0 for the OKG of quartz glass. And the intensities of the images for the bismuth–plumbum oxide glass were approximately two orders of magnitude higher than that for the quartz glass. The experimental results indicated that the bismuth–plumbum oxide glass was an excellent optical material for nonlinear optical applications.

Keywords: Bismuth–plumbum oxide glass; optical Kerr gate; ballistic imaging

PACS numbers: 06.60.Jn, 42.65.Hw, 42.68.Mj, 42.70.Mp

1. Introduction

During the last years, nonlinear optical materials have attracted an extensive attention of the scientific community due to their potential applications in photonic and optoelectronic technologies [1–4]. Therefore, various materials, such as inorganic glasses [5], organic or polymeric materials [6,7], and semiconductors [8] have been prepared via different methods. Among these various promising optical materials, oxide glasses containing heavy atomic (ionic) oxides, such as bismuthate, tellurite, or plumbum oxides, have stimulated great interest because they have the advantages of high chemical and thermal stability, simple fabrication process, low optical loss over large spectral ranges, and high optical damage threshold [9–12]. Particularly, many bismuth-based glasses with heavy atomic (ionic) oxides present large third-order optical nonlinearities for the applications in ultrafast all-optical switches [13], optical power limiters [14], and wavelength division multiplexing devices [15].

Recently, it was reported that the optical Kerr-gated (OKG) ballistic imaging employed a short time gate to visualize the object hidden in turbid media by selecting the ballistic and snake photons, and suppressing scattering photons, which were applied in investigating the characterization of turbid media such as biological tissue [16], fuel sprays [17], and liquid jets [18]. Recently, we demonstrated time-gated ballistic imaging using $SrTiO_3$ crystals and time-resolved shape measurements using bismuth–boron oxide glasses [4,8,19], in which we found that comparing with $SrTiO_3$ crystals the bismuth-based glasses with heavy atomic (ionic) oxides have the larger hyperpolarizability and ultrafast response time, so they can be expected to be promising nonlinear optical materials for time-gated ballistic imaging.

In this paper, we presented the study of nonlinear optical properties of heavy atomic oxide glasses that contained high concentrations of bismuth and plumbum. The third-order nonlinear refractive index n_2 of the bismuth–plumbum oxide glass was measured to be 2.19×10^{-15} cm^2/W, and the nonlinear response time was estimated to be shorter than 180 fs. For its application, we investigated the time-gated ballistic imaging using the bismuth–plumbum oxide glass as the Kerr medium. In the experiment, the contrasts and intensities of the images for the bismuth–plumbum oxide glass were higher than that for the quartz glass.

2. Nonlinear optical property of the bismuth–plumbum oxide glass

In the experiment, the chemical compositions of the bismuth–plumbum oxide glass were Bi_2O_3 (52 wt%), PbO (17 wt%), B_2O_3 (23 wt%), Sb_2O_3 (4 wt%), and SiO_2 (4 wt%). The fabricating craft and optical properties of bismuth–plumbum oxide glass are given in Ref. [20]. The thicknesses of both bismuth–plumbum oxide glass

*Corresponding author. Email: tanwenjiang@mail.xjtu.edu.cn

and quartz glass were 2 mm. Using the optical Kerr effect method, we measured the nonlinear optical property of the bismuth–plumbum oxide glass. Figure 1(*a*) shows the normalized time-resolved optical Kerr signals for the bismuth–plumbum oxide glass and quartz glass. The hollow squares and the solid squares refer to bismuth–plumbum oxide glass and quartz glass, respectively. The third-order nonlinear coefficient n_2 of the bismuth–plumbum oxide glass was calculated with the following formula $n_{2,B} = n_{2,R}\,(I_B/I_R)^{1/2}$, where I is the OKG signal intensity, and the subscripts of the B and R indicate for bismuth–plumbum oxide glass and the reference sample of quartz glass, respectively [13,21]. The OKG signal intensity of bismuth–plumbum oxide glass was about 78 times larger than that of quartz glass. Comparing with the third-order nonlinear refractive index for quartz glass of 2.48×10^{-16} cm^2/W, the third-order nonlinear coefficient n_2 of the bismuth–plumbum oxide glass was estimated to be 2.19×10^{-15} cm^2/W. The full width at half-maximum (FWHM) of the time-resolved optical Kerr signals for both materials was about 180 fs in Figure 1(*a*), which showed symmetric profiles without slow decay components. These results indicated that the dominant mechanism of nonlinearity for bismuth–plumbum oxide glass was attributed to electronic polarization due to the femtosecond response time [22]. It should be indicated that the nonlinear response time of the bismuth–boron oxide glass has been measured to be less than 85 fs [19], and the 180 fs FWHM measured here can be attributed to laser pulses broadened by the complex elements in the ballistic imaging system. Figure 1(*b*) shows the pump power dependence of optical Kerr signals at 780 nm for the bismuth–plumbum oxide glass and the quartz, respectively. For the sake of comparison, the curve of the signal intensity for quartz glass was magnified in the inset of Figure 1(*b*). When the gating intensity is the same, the OKG signal intensity of bismuth–plumbum oxide glass was measured to be about 80 times larger than that of quartz glass. This result is consistent with the measurement results of n_2 for bismuth–plumbum oxide glass and quartz glass, thus confirming the optical Kerr signals.

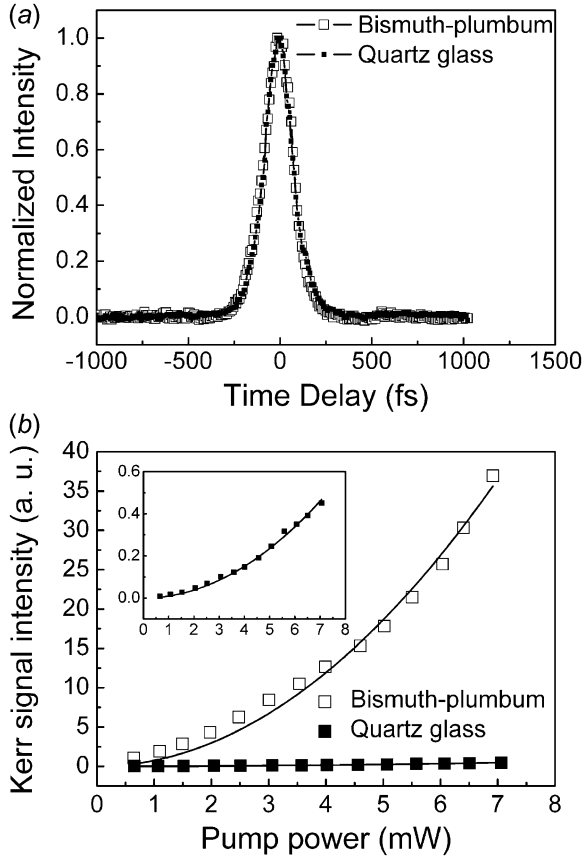

Figure 1. Optical Kerr signal measurements for the bismuth–plumbum oxide glass and the quartz glass: (*a*) normalized time-resolved optical Kerr signal, (*b*) pump power dependence of optical Kerr signals and the curve of quartz glass was magnified in the inset.

3. Time-gated ballistic imaging using OKG of the bismuth–plumbum oxide glass

Figure 2 shows the experimental setup for the ballistic imaging system scheme. A Ti: sapphire laser system (Coherent Inc., Libra-USP-HE) emitting 50 fs laser pulses, which centered at 800 nm at a repetition rate of 1 kHz, was used in our experiments. In time-gated ballistic imaging, two-color pump-probe arrangement (as the

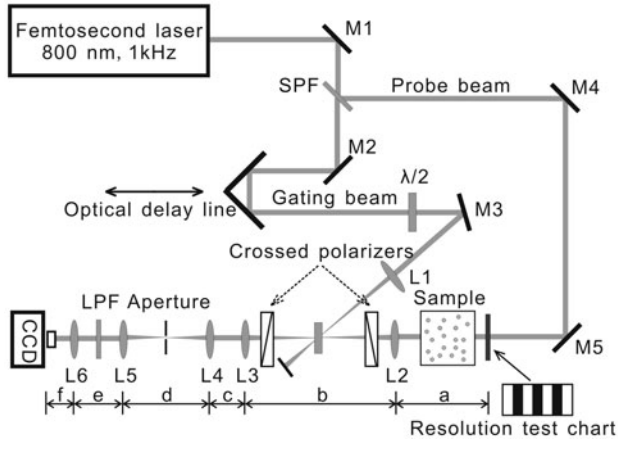

Figure 2. Experimental setup scheme of the time-gating ballistic imaging system. SPF, short-pass filter; $\lambda/2$, half-wave plate; M: mirror; LPF, long-pass filter; L1, L2, L3, L4, L5, and L6, lenses with focal lengths of 180, 150, 100, 100, 100, and 160 mm, respectively. All the diameters of the lenses were 50 mm, and $a = 150$ mm, $b = 250$ mm, $c = 80$ mm, $d = 200$ mm, $e = 215$ mm, $f = 45$ mm.

frequency doubling scheme) was usually performed to improve the signal-to-noise ratio. However, double-frequency pulses of the 800-nm laser could be seriously absorbed by the bismuth–plumbum oxide glass. In our experiment, the output of the laser beam was split into two beams by a short pass filter (SPF: Newport Inc., 10SWF-800-B). The central wavelengths of the two beams were about 780 nm and 800 nm, respectively. Passing through a variable optical delay line, the short wavelength part was focused onto an optical Kerr medium as the gating beam by a lens (L1). A half-wave plate was introduced into the gating beam to make the angle of the polarizations between the pump and the probe beams to be $\pi/4$ for the maximum gating efficiency.

The long wavelength part was reflected by the SPF and passed through a turbid sample media as the probe beam, which was modulated by a resolution test pattern (a United States Air Force contrast target) before the sample cell. The disturbed imaging beam was collected by L2 and passed through the OKG which consisted of a pair of polarizers and a Kerr material between them. By adjusting the optical delay line, ballistic photons can be gated by the OKG. Then the ballistic photons were collected by a lens (L3) and passed through a spatial filter which was composed of two 10-mm-focal-length lenses (L4 and L5) with a 1-mm-diameter aperture at the focal plane. A long-pass filter (LPF: Newport Inc., 10LWF-800-B) was inserted before the high resolution CCD camera (Lumenera Inc., INFINITY 3–1), which was used to eliminate noise photons generated by the gating beam scattering in the Kerr medium. In the experiment, the turbid media were monodisperse Polymethylmethacrylate (PMMA) microspheres suspensions with a mean diameter of 15 μm in deionized water. And the turbid media were filled in a 5-cm path-length sample cell. The optical densities (ODs) of different turbid media were controlled by adjusting the concentrations of PMMA microspheres suspensions and measured by the collimated transmittance method with a detection acceptance angle of 0.16° [23].

Because of the large nonlinearity and fast response time, bismuth–plumbum oxide glass was used as the OKG medium in the ballistic imaging. Figure 3 shows a typical imaging result. Without the OKG and the turbid media, the object was direct imaged and shown in Figure 3(*a*). Figure 3(*b*) shows the image of the object hidden in the turbid media without the OKG. The OD of the turbid media was measured to be 8.6. Without using the OKG, the image of the object is seriously disturbed. Figure 3(*c*) shows the time-gated ballistic image using the OKG. From Figure 3(*b*) and (*c*), we found that the time-gated ballistic imaging greatly improved the visualization of the object.

To further evaluate the performance of the ballistic imaging, we calculated the contrast of images in Element 5 section at different ODs by varying the concentration of the turbid media, as shown in the box of the Figure 3(*c*). The contrast of images was calculated with the following formula $Contrast = (I_{max} - I_{min})/(I_{max} + I_{min})$, where I_{max} is the average image intensity of the unshadowed parts in the square-wave pattern region and the I_{min} is the average image intensity of the shadowed parts in the square-wave pattern region.

Figure 4(*a*) shows the contrasts of the images with or without the OKG. The ODs were 6.1, 6.7, 7.2, 7.9, 8.1, 8.6, 9.1, and 9.3 for bismuth–plumbum glass, and 5.8, 6.2 6.7, and 7.0 for quartz glass. From Figure 4(*a*), we can see that the contrasts of images using the OKG varied from 0.85 to 0.5 with increasing the ODs of the turbid media. However, the maximum contrast of images without OKG was only 0.06 at OD = 6.1. The contrasts of images using the OKG were much higher than that without the OKG because the OKG can effectively eliminate the scattered photons. These results indicated that ballistic imaging using the OKG was an effective method to improve the visualization of objects hidden in the turbid media. From Figure 4(*a*), we also can see that although the contrast of the images measured using the OKG of the quartz glass was quite high, it could not improve the visualization of objects for large OD, which can be explained as follows. With increase in the OD of

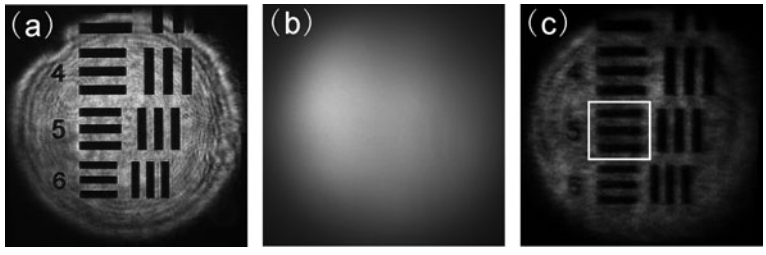

Figure 3. Comparison of the images of object under the different conditions: (*a*) without the turbid media and the OKG, (*b*) with the turbid media and without the OKG, and (*c*) with the turbid media and using the OKG of bismuth–plumbum oxide glass.

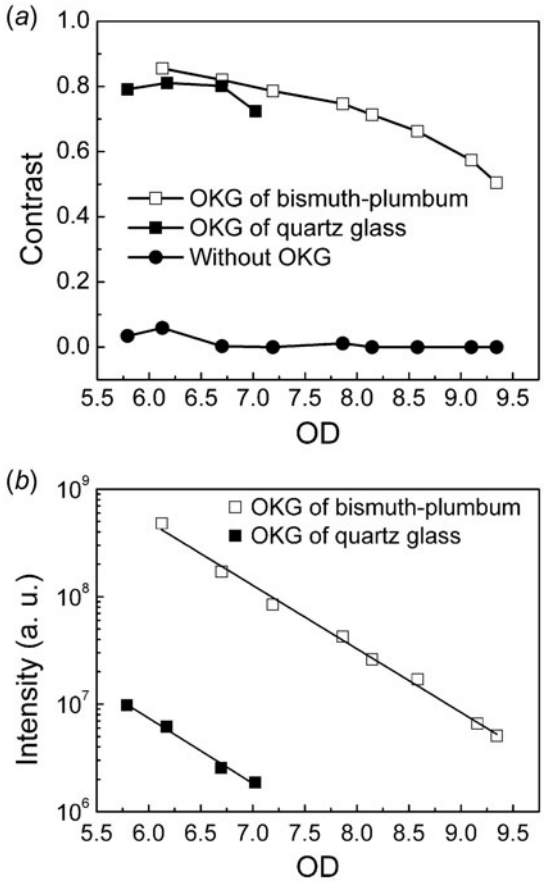

Figure 4. Comparison of the images of object at different ODs of the turbid media: (*a*) contrasts of images with or without the OKG, (*b*) signal intensities for the bismuth–plumbum oxide glass and quartz glass.

the turbid media, the signal intensity decreased and when OD was increased to more than 7, it could not reach the sensitivity limitation of the CCD camera because the nonlinear transmission of the OKG for the fused quartz was small compared to the bismuth–plumbum oxide glass.

To clearly show the different signal intensities as mentioned above, the natural logarithmic signal intensity vs. OD are shown in Figure 4(*b*). From Figure 4(*b*), we can see that the signal intensities for the bismuth–plumbum oxide glass were approximately two orders of magnitude higher than that for the quartz glass at the same OD. Thus the maximum measurable OD for the bismuth–plumbum oxide glass was about 9.3 but only about 7.0 for the quartz glass. Moreover, the signal intensity vs. OD agree well with the Beer–Lambert relation, $\mathrm{OD} = -\ln(I/I_0)$ [24], indicating that the scattering photons were eliminated efficiently by the OKG in our experiments. Here, I was the transmitted ballistic-photons intensity (without any scatting) and I_0 was the incident light intensity.

4. Conclusion

In conclusion, we have investigated the ultrafast nonlinear optical properties of the bismuth–plumbum oxide glass using the OKG method. The nonlinear refractive index n_2 of the bismuth–plumbum oxide glass was measured to be $2.19 \times 10^{-15}\,\mathrm{cm^2/W}$, and the nonlinear response time was shorter than 180 fs. Using this glass as the optical Kerr medium, we have investigated the time-gated ballistic imaging technique based on the femtosecond OKG, and the contrasts of images were higher. Because of the excellent optical nonlinearity of the bismuth–plumbum oxide glass, the intensities of images were larger than those for the quartz glass at the same OD. The maximum measurable OD using OKG of bismuth–plumbum glass was 9.3, while only 7.0 for the OKG of quartz glass in our experiment. These results indicated that the bismuth–plumbum oxide glass was an excellent OKG medium for time-gated ballistic imaging.

Funding

This work was supported by the National Science Foundation of China [grant number 61235003], [grant number 61205129]; the National Basic Research Program of China (973 Program) [grant number 2012CB921804]; the Natural Science Basic Research Plan in Shaanxi Province of China [grant number 2012JQ8002]; the Fundamental Research Funds for the Central Universities.

References

[1] Peng, M.; Qiu, J.; Chen, D.; Meng, X.; Yang, I.; Jiang, X.; Zhu, C. *Opt. Lett.* **2004,** *29,* 1998–2000.
[2] Symes, D.R.; Wegner, U.; Ahlswede, H.-C.; Streeter, M.J.V.; Gallegos, P.L.; Divall, E.J.; Smith, R.A.; Rajeev, P.P.; Neely, D. *Appl. Phys. Lett.* **2010,** *96,* 011109-1–011109-3.
[3] Tatsuura, S.; Furuki, M.; Sato, Y.; Iwasa, I.; Tian, M.; Mitsu, H. *Adv. Mater.* **2003,** *15,* 534–537.
[4] Tan, W.J.; Yang, Y.; Si, J.H.; Tong, J.Y.; Yi, W.H.; Chen, F.; Hou, X. *J. Appl. Phys.* **2010,** *107,* 043104-1–043104-3.
[5] Zhou, Z.H.; Nasu, H.; Hashimoto, T.; Kamiya, K. *J. Non-Cryst. Solids* **1997,** *215,* 61–67.
[6] Liaros, N.; Bourlinos, A.B.; Zboril, R.; Couris, S. *Opt. Express* **2013,** *21,* 21028–21038.
[7] Kang, I.; Krauss, T.D.; Wise, F.W.; Aitken, B.G.; Borrelli, N.F. *J. Opt. Soc. Am. B* **1995,** *12,* 2053–2059.
[8] Wu, B.; Tan, W.J.; Liu, X.; Si, J.H.; Zhan, P.P.; Yan, L.H.; Chen, F.; Hou, X. *Laser Phys. Lett.* **2013,** *10,* 055407-1–055407-5.
[9] Romanov, A.N.; Fattakhova, Z.T.; Zhigunov, D.M.; Korchak, V.N. *Opt. Mater.* **2011,** *33,* 631–634.
[10] Chen, F.; Xu, T.; Dai, S.; Nie, Q.; Shen, X.; Zhang, J.; Wang, X. *Opt. Mater.* **2010,** *32,* 868–872.
[11] Vithal, M.; Nachimuthu, P.; Banu, T.; Jagannathan, R. *J. Appl. Phys.* **1997,** *81,* 7922–7926.
[12] Manzani, D.; de Araújo, C.B.; Boudebs, G.; Messaddeq, Y.; Ribeiro, S.J.L. *J. Phys. Chem. B* **2013,** *117,* 408–414.

[13] Tan, W.J.; Zhou, Z.G.; Lin, A.X.; Si, J.H.; Tong, J.Y.; Hou, X. *Opt. Commun.* **2013,** *291,* 337–340.
[14] Oliveira, T.R.; Menezes, L.S.; Falcão-Filho, E.L.; Gomes, A.S.L.; de Araújo, C.B. *Appl. Phys. Lett.* **2006,** *89,* 211912-1–211912-3.
[15] Sugimoto, N. *J. Am. Ceram. Soc.* **2002,** *85,* 1083–1088.
[16] Selb, J.; Joseph, D.K.; Boas, D.A. *J. Biomed. Opt.* **2006,** *11,* 044008.
[17] Linne, M.; Sedarsky, D.; Meyer, T.; Gord, J.; Carter, C. *Exp. Fluids* **2010,** *49,* 911–923.
[18] Linne, M.; Paciaroni, M.; Gord, J.R.; Meyer, T.R. *Appl. Opt.* **2005,** *44,* 6627–6634.
[19] Tan, W.J.; Tong, J.Y.; Si, J.H.; Yang, Y.; Yi, W.H.; Chen, F.; Hou, X. *Photo. Tech. Lett.* **2011,** *23,* 471–473.
[20] Peng, M.; Zhao, Q.; Qiu, J.; Wondraczek, L. *J. Am. Ceram. Soc.* **2009,** *92,* 542–544.
[21] Yu, B.L.; Xia, H.P.; Zhu, C.S.; Gan, F.X. *Appl. Phys. Lett.* **2002,** *81,* 2701–2703.
[22] Boyd, R.W. *Nonlinear Optics 211*; Elsevier: Singapore, 2008.
[23] Michels, R.; Foschum, F.; Kienle, A. *Opt. Express* **2008,** *16,* 5907–5925.
[24] Calba, C.; Méès, L.; Rozé, C.; Girasole, T.J. *Opt. Soc. Am. A* **2008,** *25,* 1541–1550.